Observation of Enhanced Oxygen Bombardment of Titan

J.H. Westlake[1], **D.G. Mitchell**[1], **J.M. Bell**[2]

[1]Johns Hopkins University Applied Physics Laboratory, 11100 Johns Hopkins Rd., Laurel, MD, USA 20723

[2]NASA Goddard Space Flight Center, Greenbelt, MD, USA 20771

Key Points:

- Cassini observations show sporadic enhancements in the energetic oxygen bombardment at Titan
- We observe an order of magnitude enhancement in energetic oxygen flux into Titan's atmosphere
- These enhancements in oxygen bombardment could affect thermospheric temperatures at Titan

Corresponding author: Joseph Westlake, joseph.westlake@jhuapl.edu

Abstract

Here we present observations and simulations of oxygen particle bombardment into Titan's thermosphere that represents a new class of upper atmospheric stimulus. We find that these large bursts of energetic oxygen ions contain sufficient energy to perturb Titan's thermosphere, if the energy is applied at the right altitude. In this study we present Cassini observations during the T20 flyby of Titan in 2006 specifically from the Cassini Magnetospheric Imaging Instrument (MIMI; *Krimigis et al.* [2004]) and the Cassini Plasma Spectrometer (CAPS; *Young et al.* [2004]). We utilize simulations using the Titan-Global Ionosphere Thermosphere Model to assess the impact of energetic oxygen bursts similar to the one observed during T20 on the thermospheric structure. We find that energy deposited higher in Titan's thermosphere has a much greater effect on the temperatures that Cassini would observe from the INMS instrument. These higher altitude energy deposition events are similar to those that occur from corotational oxygen and water group ions in Saturn's magnetosphere. We find that the more energetic heavy ions tend to penetrate deeper into the thermosphere resulting in a much more benign heating rate and minimal temperature change, however when these events carry along lower energy thermal oxygen ions that will deposit energy at higher altitudes the temperature change can be much more substantial.

1 Introduction

Titan is constantly bombarded by Saturn's magnetospheric plasma. Saturn's outer magnetosphere, which consists primarily of protons and water group ions sourced by the plumes of Enceladus and accelerated in the inner magnetosphere, is a variable environment with several distinct types of plasmas (e.g. *Thomsen et al.* [2010]; *Rymer et al.* [2009]; *Garnier et al.* [2010]; *Simon et al.* [2010]; *Smith and Rymer* [2014]). This plasma heats and ionizes Titan's upper atmosphere and in some cases shows effects that are observed in the density structure of the thermosphere and exosphere (*Westlake et al.* [2011]; *Snowden et al.* [2013a]; *Cui et al.* [2011]). *Westlake et al.* [2011] indicated that on at least one pair of passes the thermospheric temperature had changed by 29K over 16 days. The causes of these heating events have been elusive. Several possible contributors were assessed by *Snowden et al.* [2013a] and *Snowden and Yelle* [2014]. Here we present here a new class of possible stimulus to the upper thermosphere that comes from intense energetic oxygen precipitation that could contain sufficient energy to perturb Titan's thermosphere.

Shah et al. [2009] studied the effects of suprathermal (energies above 10 keV) O^+ ion bombardment on Titan's primarily N_2 atmosphere finding that the O^+ energy deposition is maximized between 900 and 1100 km altitude. The energy deposited into Titan's thermosphere could vary by several orders of magnitude based on the energy content of the O^+. Energy deposition analyses by several authors have shown that energetic protons penetrate deep into the atmosphere depositing their energy near 700-800 km (*Luna et al.* [2003]; *Smith et al.* [2009]), while magnetospheric oxygen ions exhibit a peak energy deposition rate between 900 and 1100 km (e.g. *Snowden and Yelle* [2014]), and electrons near or above 1200 km (*Richard et al.* [2011]; *Snowden et al.* [2013b]). Time dependent simulations of the thermospheric response have shown that the thermosphere can respond to this type of stimulus with time constants that are on the order of one Titan day (16 Earth days; *Bell et al.* [2011]).

In this study we present Cassini observations during the T20 flyby of Titan. We detail observations from the Cassini Magnetospheric Imaging Instrument (MIMI; *Krimigis et al.* [2004]) and the Cassini Plasma Spectrometer (CAPS; *Young et al.* [2004]). We use these observations to model how this energetic and thermal oxygen precipitation will affect the thermospheric density structure using the Titan Global Ionosphere Thermosphere Model (T-GITM; *Bell et al.* [2010]).

2 Observations

The T20 flyby occurred on day 298 of 2006 at a local time of about 02:00, which is well into Saturn's magnetotail. Just prior to this flyby a large burst of oxygen ENAs were observed emanating from Titan's atmosphere and exosphere as shown in the time-series of INCA observations in Figure 1. The time-series shows INCA images of the flyby with the individual energy channels representing each row in the figure and the columns as roughly 3 minute time steps between 15:08 and 15:47. The oxygen ENA intensities grow as Cassini approaches Titan with the greatest intensities occurring at about 15:30 then falling back fairly rapidly (over about 10 minutes) to more commonly seen intensities. The INCA observed oxygen burst spans about 30 minutes worth of observations with intensities increasing by over two orders of magnitude. This burst of oxygen ENAs is one of the largest observed by Cassini throughout the Titan encounters. The line plot of ENA intensities through the flyby shows that the oxygen ion spectrum extends from tens to hundreds of keV with intensities that are similar to the ambient oxygen ions.

Prior to the ENA observations INCA was in ion mode with its ion deflection plates off. During this period INCA observed a significant and nearly isotropic population of oxygen ions until it switched to ENA mode at 14:45. This type of isotropic energetic oxygen ion population is fairly common in the INCA data out near Titan. *DiFabio et al.* [2011] studied the water group ion densities from 2005 to 2011 inside of 15 R_S showing that between 27 and 220 keV/e the water group ions are the dominant ion species and that their densities are basically constant over this time period. Outside of 15 R_S the Cassini coverage is much sparser and systematic studies have not been done of this data. *Sergis et al.* [2009] also showed that near 15 R_S the energetic O^+ pressure dominates and that the O^+ pressure is highly correlated with the H^+ pressure. *Sergis et al.* [2009] also showed that there is a region inside of about 20 R_S of higher particle pressure, which means that Titan sits at the edge of this high pressure region.

The decline in oxygen ENA intensity after 15:30 appears to be due to a decline in the oxygen ion intensity at Titan. This decline could also be partially due to Cassini being too close to Titan to fully image the ENAs from the full disc, or from Cassini entering Titan's extended atmosphere which will shield some ENAs. After 16:20 the O^+ ENA level has come back down to background intensities. ENA shadowing effects are common occurrences, but they generally result in specific shapes to the ENA emission from Titan (e.g. *Brandt et al.* [2012]; *Wulms et al.* [2010]) and not a full reduction in the emission. In addition the several order of magnitude decline in ENA intensity in the two frames after the peak are inconsistent with simply Titan's atmosphere or disc occulting the source. *Simon et al.* [2013] classified this flyby as in the plasma sheet on the inbound portion of the flyby and then transitioned to the southern lobe after the flyby. It appears that this drop in the O ENA emissions is consistent with a reduction of ion input at Titan due to its movement from the plasma sheet to the lobe. It is particularly interesting on this flyby that the plasma sheet appears significantly enhanced in energetic oxygen as compared to other Titan encounters.

We identify oxygen ENAs with INCA by their observed pulse-height spectrum on the MCP shown in Figure 2. The pulses observed on the stop MCP are composition dependent with heavier ions producing larger pulses than protons [Krimigis et al. 2004]. The pulse height is plotted versus the observed energy with a statistical oxygen/hydrogen separator line. The lower right portion of the plot (lower energy, high pulse-height) is the region dominated by O^+ while protons dominate the upper portion of the plot. This also shows that the O^+ ENAs are likely contaminating proton channels during this time as well. The actual com-

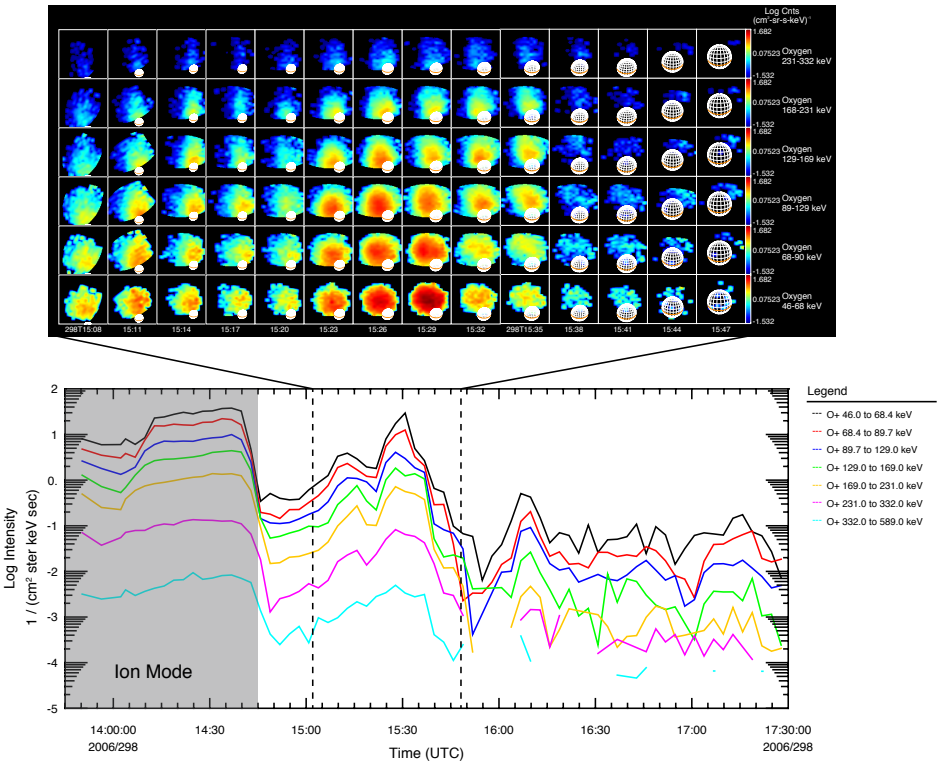

Figure 1. Oxygen ENAs observed by Cassini INCA during the T20 encounter. The top time series shows the spatial distribution of oxygen ENAs about Titan in six energy channels. Each row in the time-series gives a different energy channel with the lowest energies at the bottom and the greatest at the top. Each column is one high-energy resolution time step for INCA and are separated by about 3 minutes. The line plot below series shows the spatially summed oxygen ENA intensity for each energy channel and provides the context for this observation.

position of the ENAs are technically identified as heavy species, not protons, and assumed to be O^+ or water group ions given the composition of the ions that have been observed both in the plasma energy range and also in the higher energy particles [e.g. *Thomsen et al.* [2010]; *DiFabio et al.* [2011]].

Cassini CAPS also saw enhancements in the lower energy water group ions prior to and during this flyby. The CAPS Ion Mass Spectrometer (IMS) data is shown in Figure 3. The energy per charge spectrogram shows two distinct peaks, which are consistent with corotating protons and water group ions that are common to Saturn's magnetosphere [*Thomsen et al.*, 2010]. There is also a prevalence of a third peak in the E/Q spectrum that is likely H_2^+,

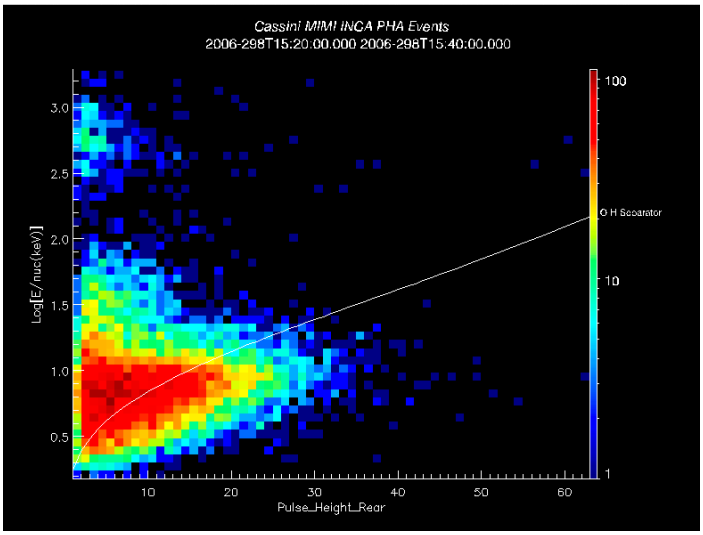

Figure 2. MIMI INCA MCP pulse height spectrum between 15:20 to 15:40. The line drawn across the plot is the statistical O/H separator with O ENAs falling below the line and H ENAs above the line. This line is statistically drawn and there will be some O ENAs above the line and some H ENAs below the line. This distribution shows that most of the events recorded are oxygen events with very little protons. It is also clear from this spectrum that the low energy proton observations are contaminated by O ENAs.

which has been shown to be present near Titan [*Thomsen et al.*, 2010]. The CAPS instrument is on an actuated platform, so the magnetospheric flow direction is only in the field of view for part of the time and hence the spotty appearance of the plasma data. In the time around 12:45 there is a very strong water group component to the magnetospheric flow, but this component appears to come and go on a fairly short timescale (about 30 minutes). As Cassini approaches Titan the water group ion feature returns and stays fairly constant from about 14:24 to 15:10 when the feature disappears. This is coincident with the enhanced period of oxygen ENAs.

3 Effect on Thermospheric Temperatures

These observations raise several questions related to the variability of Titan's thermosphere and exosphere such as how frequent are these oxygen bursts at Titan and what are their effect on the thermospheric temperatures? We first address the effect of the oxygen burst on the thermospheric temperatures using the T-GITM model run in its time-dependent mode [*Bell et al.*, 2011]. The model was run in a 1-D mode for three years with low and constant heating to produce a stable equilibrium. The atmosphere was then given the pulse of

energy deposition with a time and altitude profile shown in 4, which is the altitude dependent energy deposition profile calculated by *Shah et al.* [2009] and a time dependence consistent with the INCA observations. The results are shown in Figure 4. The inclusion of this additional energy deposition minimally changes the thermospheric temperature with little to no change in the temperature at 1000 km altitude and roughly one degree increase at 1400 km altitude. We attribute this to the fairly long timescales low in Titan's atmosphere where most of the energy is deposited from the high energy oxygen. The oxygen ion precipitation would have to persist for several hours to days to have a substantial effect on the thermospheric temperatures at 1000 km.

If the heating pulse occurs at a higher altitude as would be the case for lower energy oxygen ions such as the water group population observed by CAPS then the heating may have a more dramatic effect on the observed temperatures at altitudes that Cassini has access to. The corotational water group ions deposit most of their energy above about 1200 km [*Snowden and Yelle*, 2014]. To simulate this case we used the simple two-dimensional Gaussian shown in Figure 5 as the heating pulse with its peak heating rate at 1300 km, and a peak energy deposition rate equal to that of the energetic oxygen ions. The results of this run are shown in Figure 5. Clearly the effect of moving the peak energy deposition altitude from 1100 km to 1300 km has a significant effect on the thermospheric temperatures above 1300 km. Our test showed a 25K increase in the thermospheric temperature at 1400 km over one hour.

Snowden and Yelle [2014] used the continuous loss approximation to calculate the energy deposition rate of thermal oxygen ions finding that they generally deposited most of their energy near 1100 km altitude with peak energy deposition rates of 68 eV cm^{-3} s^{-1} and that the more energetic oxygen ions deposited 22 eV cm^{-3} s^{-1} at a peak altitude of 980 km. These values have a 50% efficiency applied to them due to the non-uniform ion flux. We note that the oxygen ions above a few tens of keV are generally isotropic out near Titan and therefore uniformly deposit energy over Titan's atmosphere [Regoli et al., 2015]. The oxygen ion fluxes used to calculate the energy deposition profile in *Snowden and Yelle* [2014] are robust but significantly smaller than those of the T20 flyby with intensities of 5 cm^{-2} sr^{-1} s^{-1} keV^{-1} at 40 keV compared to the peak observed oxygen ion flux during the T20 flyby of 60 cm^{-2} sr^{-1} s^{-1} keV^{-1}. The spectrum used for the *Snowden and Yelle* [2014] calculations are more reflective of the average situation at Titan. We therefore believe that the peak energy deposition rates used in this modeling effort (300 cm^{-2} sr^{-1} s^{-1} keV^{-1}) are consistent with

the roughly order of magnitude or greater increase in oxygen ion fluxes observed during this flyby.

The enhancement in oxygen ENAs do not occur without coincident enhancements in hydrogen ENAs and possibly also energetic electron enhancements, which would add additional energy deposition. As was shown by *Sergis et al.* [2009] the O^+ particle pressure correlates with the H^+ particle pressure. If the ion pressures increase due to a density increase then the resultant ENAs will also increase. Particle pressure can change either due to density changes or due to temperature changes. Temperature changes in the plasma will change both the energy deposition at Titan and also the ENA observations as the charge-exchange cross section is highly dependent on the particle energy. The enhanced O ENAs observed during this encounter appears consistent with changes in the O^+ density, therefore we expect the H^+ and electron densities to also increase. These increases in densities at Titan will result in enhanced energy input into Titan's thermosphere over what was estimated for O^+ bombardment alone.

4 Conclusions

We have presented an observation of greatly enhanced oxygen ion and ENA fluxes near Titan. The enhanced thermal and energetic ions are seen by the Cassini CAPS and MIMI instruments and show roughly an order of magnitude greater intensities than the nominal conditions at Titan. These oxygen ions clearly impact Titan's atmosphere producing copious oxygen ENAs that were observed by Cassini INCA. This oxygen burst was clearly an energetic event that had sufficient energy to effect Titan's thermospheric temperatures.

We evaluated the effect of the enhanced thermospheric energy deposition using the time-dependent T-GITM model. We showed that the very energetic oxygen ions had little effect on temperatures in the lower thermosphere near the homopause at 1000 km due to the long timescales of the atmosphere and the relatively short duration of these oxygen ion bursts. We also showed that energy deposition applied at higher altitudes such as that given by thermal oxygen ions had a much more substantial effect at higher altitudes with a potential temperature change of up to 25K over one hour.

Acknowledgments

This work was supported by NASA Grant 80NSSC20K0378 from the NASA Cassini Data Analysis program as well as the Cassini MIMI subcontract from JPL before the end of the Cassini mission.

References

Bell, J. M., S. W. Bougher, J. H. Waite, A. J. Ridley, B. A. Magee, K. E. Mandt, J. Westlake, A. D. DeJong, A. BarâĂŞNun, R. Jacovi, G. Toth, and V. De La Haye (2010), Simulating the one-dimensional structure of Titan's upper atmosphere: 1. Formulation of the Titan Global Ionosphere-Thermosphere Model and benchmark simulations, *Journal of Geophysical Research: Planets*, *115*(E12), E12,002, doi:10.1029/2010JE003636.

Bell, J. M., J. Westlake, and J. H. Waite (2011), Simulating the time-dependent response of Titan's upper atmosphere to periods of magnetospheric forcing, *Geophysical Research Letters*, *38*(6), n/a–n/a, doi:10.1029/2010GL046420.

Brandt, P. C., K. Dialynas, I. Dandouras, D. G. Mitchell, P. Garnier, and S. M. Krimigis (2012), The distribution of Titan's high-altitude (out to âĹij50,000 km) exosphere from energetic neutral atom (ENA) measurements by Cassini/INCA, *Planetary and Space Science*, *60*(1), 107–114, doi:10.1016/j.pss.2011.04.014.

Cui, J., R. V. Yelle, I. C. F. MÃijller-Wodarg, P. P. Lavvas, and M. Galand (2011), The implications of the H2 variability in Titan's exosphere, *Journal of Geophysical Research: Space Physics*, *116*(A11), A11,324, doi:10.1029/2011JA016808.

DiFabio, R. D., D. C. Hamilton, S. M. Krimigis, and D. G. Mitchell (2011), Long term time variations of the suprathermal ions in Saturn's magnetosphere, *Geophysical Research Letters*, *38*(18), L18,103, doi:10.1029/2011GL048841.

Garnier, P., I. Dandouras, D. Toublanc, E. Roelof, P. Brandt, D. Mitchell, S. Krimigis, N. Krupp, D. Hamilton, and J.-E. Wahlund (2010), Statistical analysis of the energetic ion and ENA data for the Titan environment, *Planetary and Space Science*, *58*(14âĂŞ15), 1811–1822, doi:10.1016/j.pss.2010.08.009.

Krimigis, S. M., D. G. Mitchell, D. C. Hamilton, S. Livi, J. Dandouras, S. Jaskulek, T. P. Armstrong, J. D. Boldt, A. F. Cheng, G. Gloeckler, J. R. Hayes, K. C. Hsieh, W.-H. Ip, E. P. Keath, E. Kirsch, N. Krupp, L. J. Lanzerotti, R. Lundgren, B. H. Mauk, R. W. McEntire, E. C. Roelof, C. E. Schlemm, B. E. Tossman, B. Wilken, and D. J. Williams (2004), Magnetosphere Imaging Instrument (MIMI) on the Cassini Mission to Saturn/Titan, *Space*

Science Reviews, *114*(1-4), 233–329, doi:10.1007/s11214-004-1410-8.

Luna, H., M. Michael, M. B. Shah, R. E. Johnson, C. J. Latimer, and J. W. McConkey (2003), Dissociation of N2 in capture and ionization collisions with fast H+ and N+ ions and modeling of positive ion formation in the Titan atmosphere, *Journal of Geophysical Research: Planets*, *108*(E4), n/a–n/a, doi:10.1029/2002JE001950.

Richard, M. S., T. E. Cravens, I. P. Robertson, J. H. Waite, J.-E. Wahlund, F. J. Crary, and A. J. Coates (2011), Energetics of Titan's ionosphere: Model comparisons with Cassini data, *Journal of Geophysical Research: Space Physics*, *116*(A9), A09,310, doi:10.1029/2011JA016603.

Rymer, A. M., H. T. Smith, A. Wellbrock, A. J. Coates, and D. T. Young (2009), Discrete classification and electron energy spectra of Titan's varied magnetospheric environment, *Geophysical Research Letters*, *36*(15), n/a–n/a, doi:10.1029/2009GL039427.

Sergis, N., S. M. Krimigis, D. G. Mitchell, D. C. Hamilton, N. Krupp, B. H. Mauk, E. C. Roelof, and M. K. Dougherty (2009), Energetic particle pressure in Saturn's magnetosphere measured with the Magnetospheric Imaging Instrument on Cassini, *Journal of Geophysical Research: Space Physics*, *114*(A2), A02,214, doi:10.1029/2008JA013774.

Shah, M. B., C. J. Latimer, E. C. Montenegro, O. J. Tucker, R. E. Johnson, and H. T. Smith (2009), The Implantation and Interactions of O+ in Titan's Atmosphere: Laboratory Measurements of Collision-induced Dissociation of N2 and Modeling of Positive Ion Formation, *The Astrophysical Journal*, *703*(2), 1947, doi:10.1088/0004-637X/703/2/1947.

Simon, S., A. Wennmacher, F. M. Neubauer, C. L. Bertucci, H. Kriegel, J. Saur, C. T. Russell, and M. K. Dougherty (2010), Titan's highly dynamic magnetic environment: A systematic survey of Cassini magnetometer observations from flybys TAâĂŞT62, *Planetary and Space Science*, *58*(10), 1230–1251, doi:10.1016/j.pss.2010.04.021.

Simon, S., S. C. van Treeck, A. Wennmacher, J. Saur, F. M. Neubauer, C. L. Bertucci, and M. K. Dougherty (2013), Structure of Titan's induced magnetosphere under varying background magnetic field conditions: Survey of Cassini magnetometer data from flybys TAâĂŞT85, *Journal of Geophysical Research: Space Physics*, *118*(4), 1679–1699, doi:10.1002/jgra.50096.

Smith, H., D. Mitchell, R. Johnson, and C. Paranicas (2009), Investigation of energetic proton penetration in Titan's atmosphere using the Cassini INCA instrument, *Planetary and Space Science*, *57*(13), 1538–1546, doi:10.1016/j.pss.2009.03.013.

277 Smith, H. T., and A. M. Rymer (2014), An empirical model for the plasma environment
278 along Titan's orbit based on Cassini plasma observations, *Journal of Geophysical Re-*
279 *search: Space Physics*, p. 2014JA019872, doi:10.1002/2014JA019872.
280 Snowden, D., and R. V. Yelle (2014), The thermal structure of TitanâĂŹs upper atmosphere,
281 II: Energetics, *Icarus*, *228*, 64–77, doi:10.1016/j.icarus.2013.08.027.
282 Snowden, D., R. V. Yelle, J. Cui, J. E. Wahlund, N. J. T. Edberg, and K. ÃĚgren (2013a),
283 The thermal structure of TitanâĂŹs upper atmosphere, I: Temperature profiles from
284 Cassini INMS observations, *Icarus*, *226*(1), 552–582, doi:10.1016/j.icarus.2013.06.006.
285 Snowden, D., R. V. Yelle, M. Galand, A. J. Coates, A. Wellbrock, G. H. Jones, and P. Lavvas
286 (2013b), Auroral electron precipitation and flux tube erosion in TitanâĂŹs upper atmo-
287 sphere, *Icarus*, *226*(1), 186–204, doi:10.1016/j.icarus.2013.05.021.
288 Thomsen, M. F., D. B. Reisenfeld, D. M. Delapp, R. L. Tokar, D. T. Young, F. J. Crary, E. C.
289 Sittler, M. A. McGraw, and J. D. Williams (2010), Survey of ion plasma parameters in
290 Saturn's magnetosphere, *Journal of Geophysical Research: Space Physics*, *115*(A10),
291 n/a–n/a, doi:10.1029/2010JA015267.
292 Westlake, J. H., J. M. Bell, J. H. Waite, R. E. Johnson, J. G. Luhmann, K. E. Mandt, B. A.
293 Magee, and A. M. Rymer (2011), Titan's thermospheric response to various plasma en-
294 vironments, *Journal of Geophysical Research: Space Physics*, *116*(A3), n/a–n/a, doi:
295 10.1029/2010JA016251.
296 Wulms, V., J. Saur, D. F. Strobel, S. Simon, and D. G. Mitchell (2010), Energetic neutral
297 atoms from Titan: Particle simulations in draped magnetic and electric fields, *Journal of*
298 *Geophysical Research: Space Physics*, *115*(A6), n/a–n/a, doi:10.1029/2009JA014893.
299 Young, D. T., J. J. Berthelier, M. Blanc, J. L. Burch, A. J. Coates, R. Goldstein, M. Grande,
300 T. W. Hill, R. E. Johnson, V. Kelha, D. J. Mccomas, E. C. Sittler, K. R. Svenes,
301 K. SzegÃűi, P. Tanskanen, K. Ahola, D. Anderson, S. Bakshi, R. A. Baragiola, B. L. Barr-
302 aclough, R. K. Black, S. Bolton, T. Booker, R. Bowman, P. Casey, F. J. Crary, D. Delapp,
303 G. Dirks, N. Eaker, H. Funsten, J. D. Furman, J. T. Gosling, H. Hannula, C. Holmlund,
304 H. Huomo, J. M. Illiano, P. Jensen, M. A. Johnson, D. R. Linder, T. Luntama, S. Maurice,
305 K. P. Mccabe, K. Mursula, B. T. Narheim, J. E. Nordholt, A. Preece, J. Rudzki, A. Ruit-
306 berg, K. Smith, S. Szalai, M. F. Thomsen, K. Viherkanto, J. Vilppola, T. Vollmer, T. E.
307 Wahl, M. WÃijest, T. Ylikorpi, and C. Zinsmeyer (2004), Cassini Plasma Spectrometer
308 Investigation, *Space Science Reviews*, *114*(1-4), 1–112, doi:10.1007/s11214-004-1406-4.

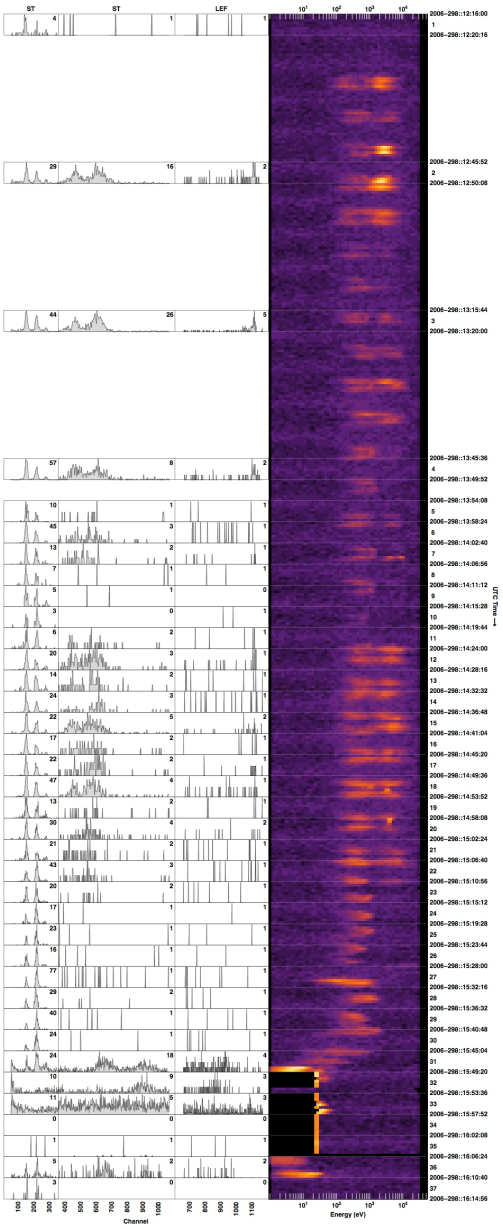

Figure 3. CAPS-IMS data from the T20 flyby. The color plot shows the energy per charge spectrogram leading up to the Titan flyby. The horizontal lines across the plot give the "B-cycle" timing of the CAPS instrument in which one composition measurement is made. The panels to the left show each time of flight measurement both in the straight through (ST) and linear electric field (LEF) modes of the instrument.

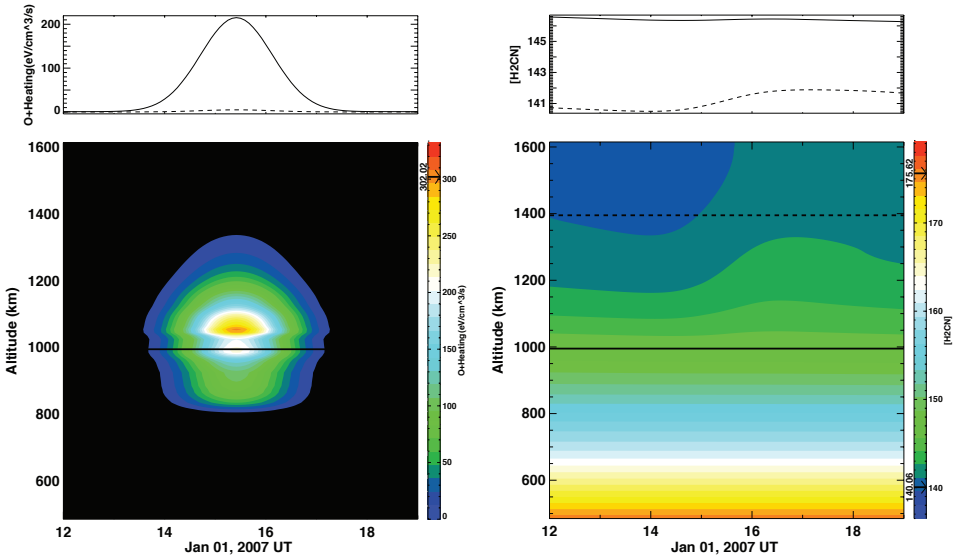

155 **Figure 4.** The left two panels show the time and altitude dependent energy deposition profile given to the
156 T-GITM model. The upper left panel shows a cut through 1000 km altitude. The right panel shows the ther-
157 mospheric temperatures during this heating pulse. The upper right plot shows a cut through the plot at 1000
158 km (solid line) and 1400 km (dashed line).

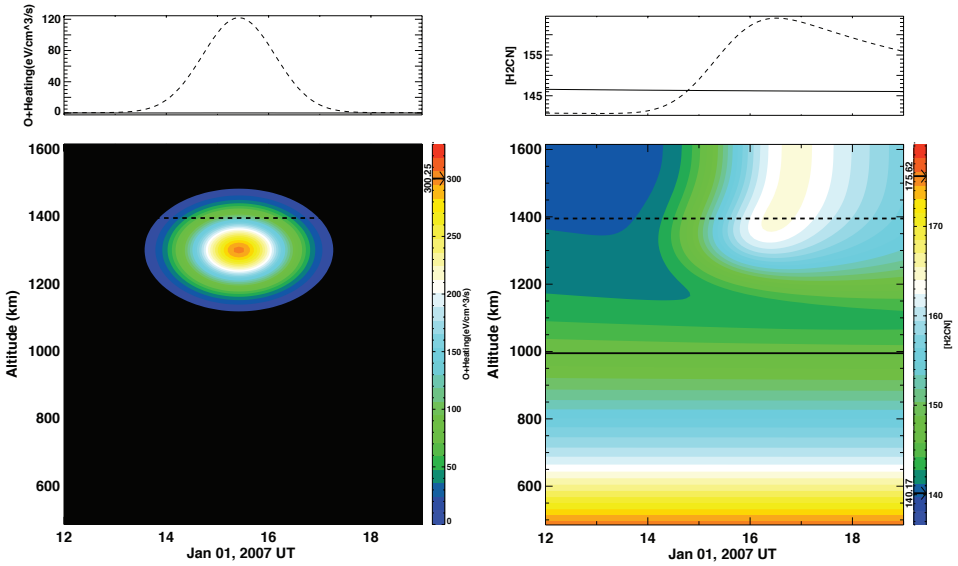

170 **Figure 5.** Same plots as Figure 4 but with a two-dimensional Gaussian heating pulse centered at 1300 km
171 altitude.

Figure 1.

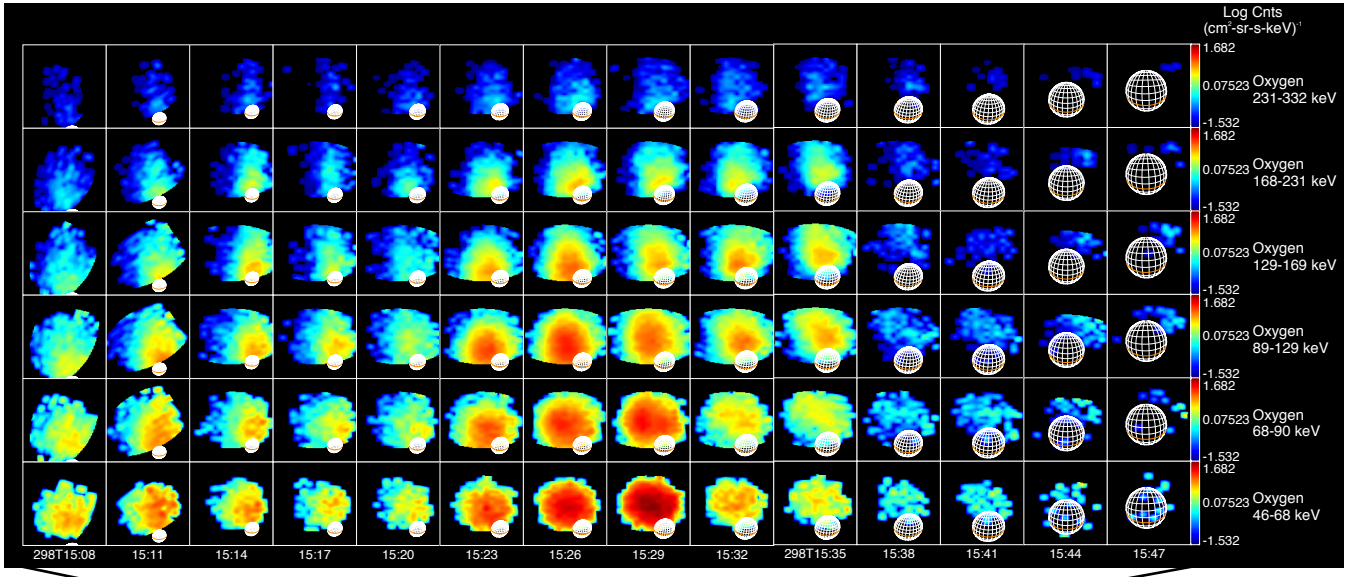
Log Cnts
(cm²-sr-s-keV)⁻¹
1.682
0.07523
-1.532
Oxygen
231-332 keV
Oxygen
168-231 keV
Oxygen
129-169 keV
Oxygen
89-129 keV
Oxygen
68-90 keV
Oxygen
46-68 keV
298T15:08
15:11
15:14
15:17
15:20
15:23
15:26
15:29
15:32
298T15:35
15:38
15:41
15:44
15:47

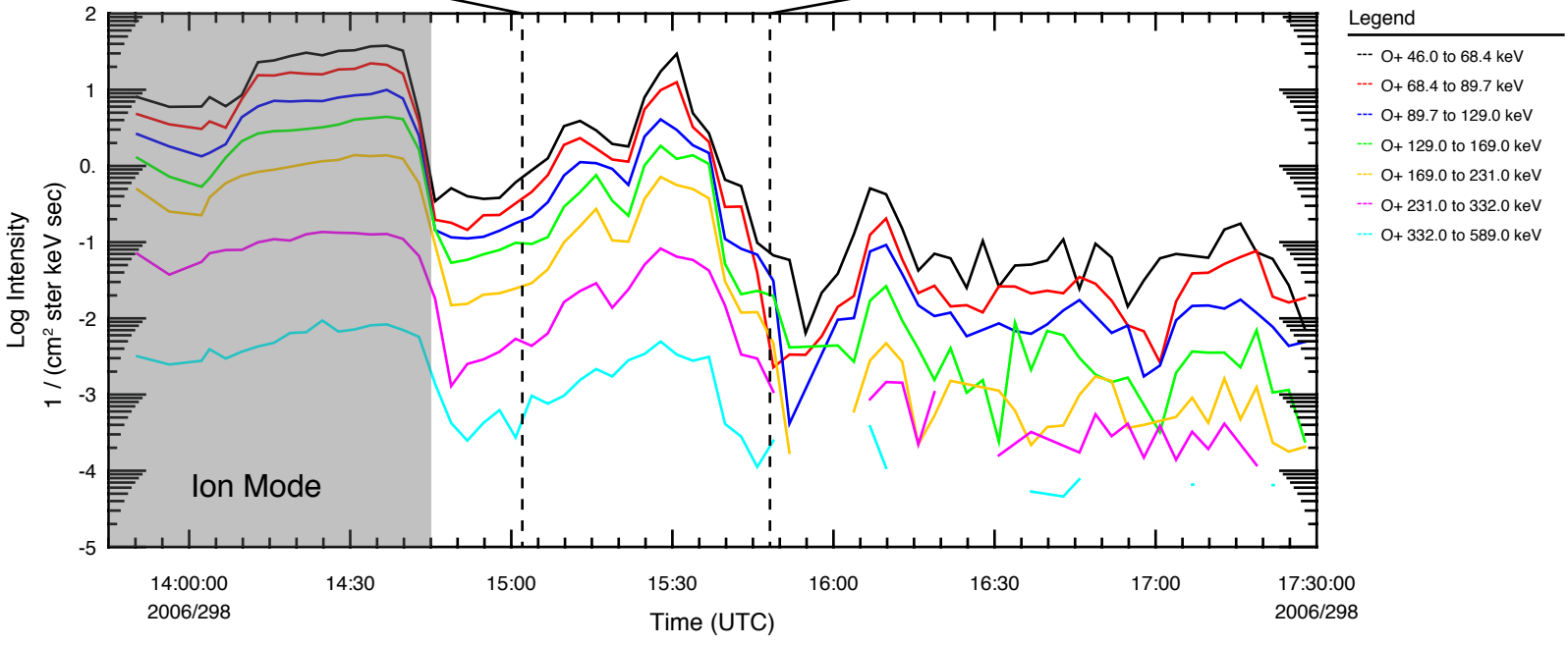
Log Intensity
1 / (cm² ster keV sec)
2
1
0.
-1
-2
-3
-4
-5
Ion Mode
14:00:00
2006/298
14:30
15:00
15:30
16:00
16:30
17:00
17:30:00
2006/298
Time (UTC)
Legend
O+ 46.0 to 68.4 keV
O+ 68.4 to 89.7 keV
O+ 89.7 to 129.0 keV
O+ 129.0 to 169.0 keV
O+ 169.0 to 231.0 keV
O+ 231.0 to 332.0 keV
O+ 332.0 to 589.0 keV

Figure 2.

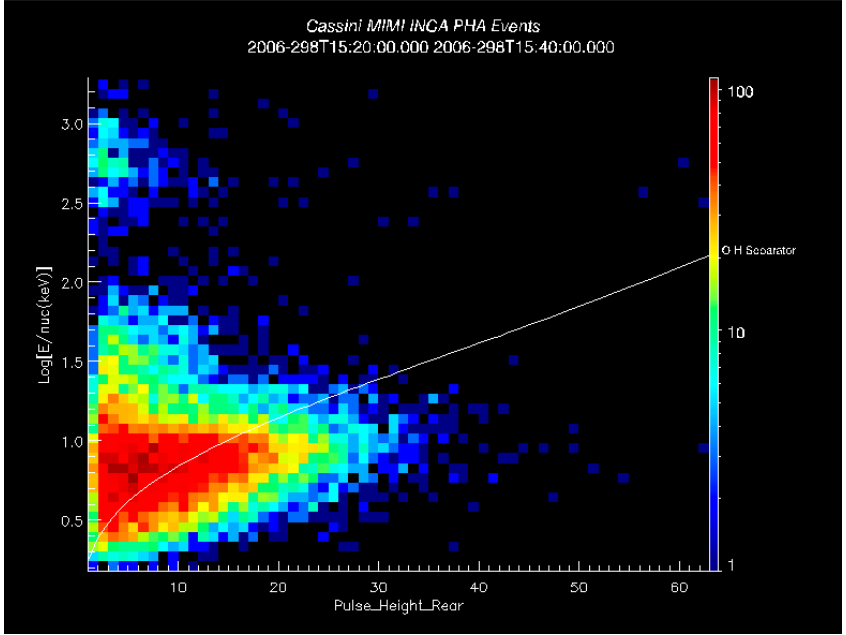
Cassini MIMI INCA PHA Events
2006-298T15:20:00.000 2006-298T15:40:00.000
Log[E/nuc(keV)]
3.0
2.5
2.0
1.5
1.0
0.5
10
20
30
40
50
60
Pulse_Height_Rear
100
O H Separator
10
1

Figure 3.

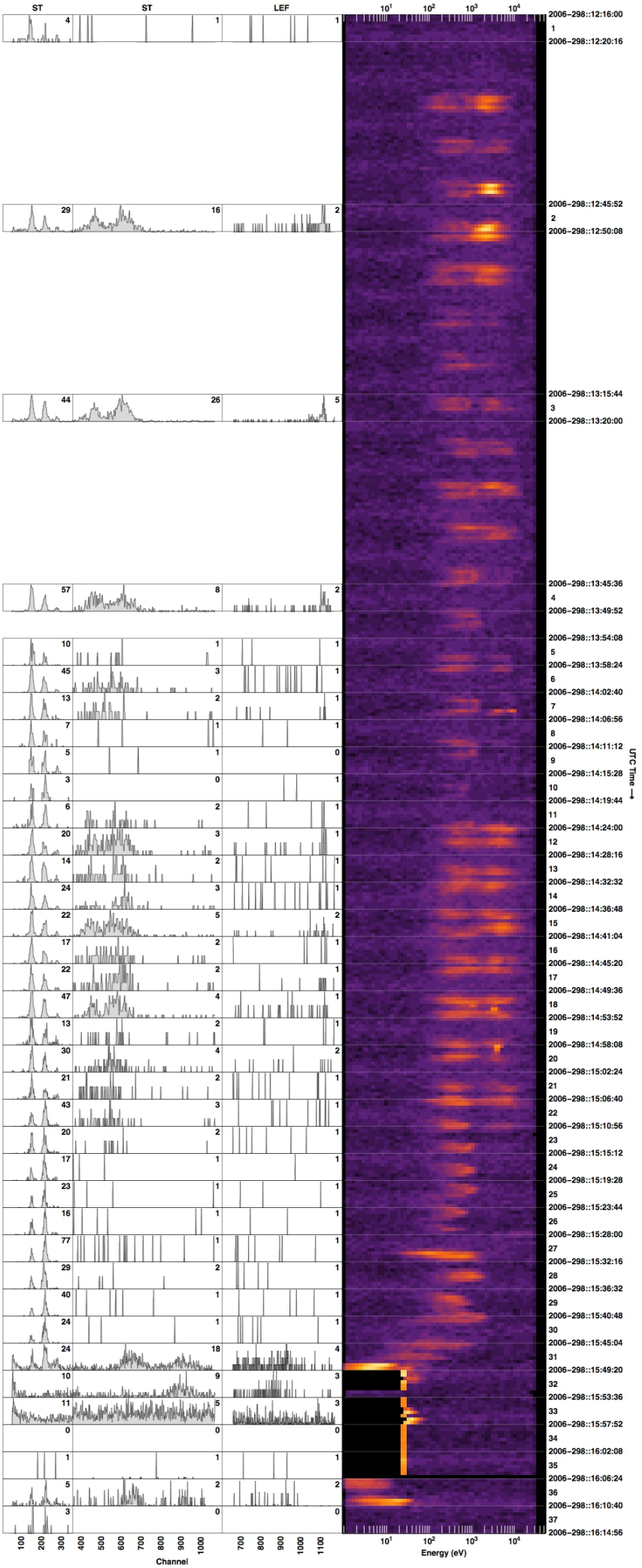
ST
ST
LEF
10^1
10^2
10^3
10^4
2006-298::12:16:00
2006-298::12:20:16
2006-298::12:45:52
2006-298::12:50:08
2006-298::13:15:44
2006-298::13:20:00
2006-298::13:45:36
2006-298::13:49:52
2006-298::13:54:08
2006-298::13:58:24
2006-298::14:02:40
2006-298::14:06:56
2006-298::14:11:12
2006-298::14:15:28
2006-298::14:19:44
2006-298::14:24:00
2006-298::14:28:16
2006-298::14:32:32
2006-298::14:36:48
2006-298::14:41:04
2006-298::14:45:20
2006-298::14:49:36
2006-298::14:53:52
2006-298::14:58:08
2006-298::15:02:24
2006-298::15:06:40
2006-298::15:10:56
2006-298::15:15:12
2006-298::15:19:28
2006-298::15:23:44
2006-298::15:28:00
2006-298::15:32:16
2006-298::15:36:32
2006-298::15:40:48
2006-298::15:45:04
2006-298::15:49:20
2006-298::15:53:36
2006-298::15:57:52
2006-298::16:02:08
2006-298::16:06:24
2006-298::16:10:40
2006-298::16:14:56
UTC Time
100
200
300
400
500
600
700
800
900
1000
700
800
900
1000
1100
Channel
10^1
10^2
10^3
10^4
Energy (eV)

Figure 4.

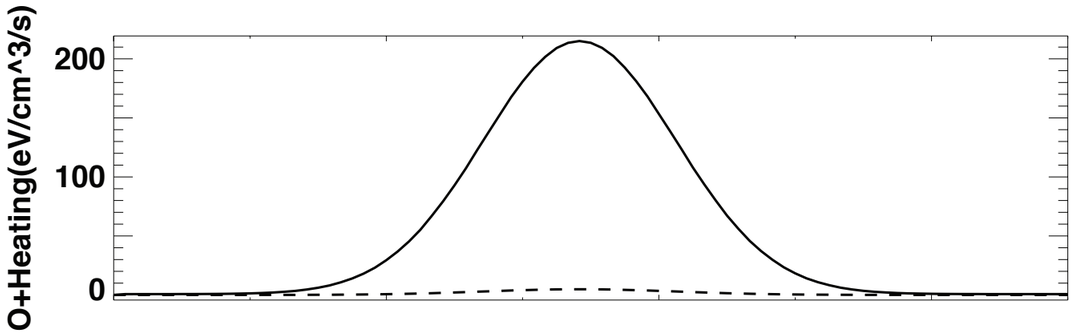
O+Heating(eV/cm^3/s)
200
100
0

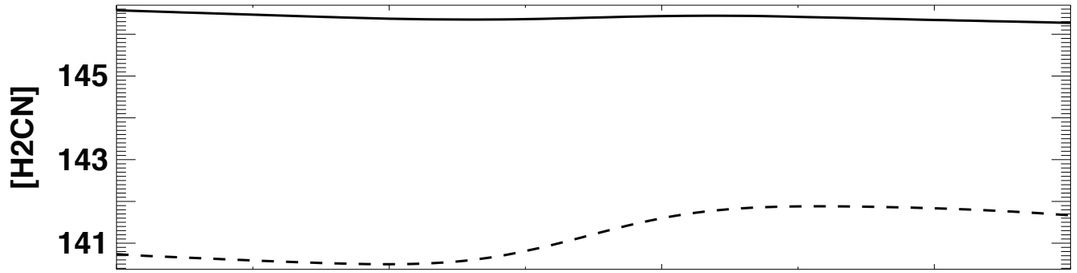
[H2CN]
145
143
141

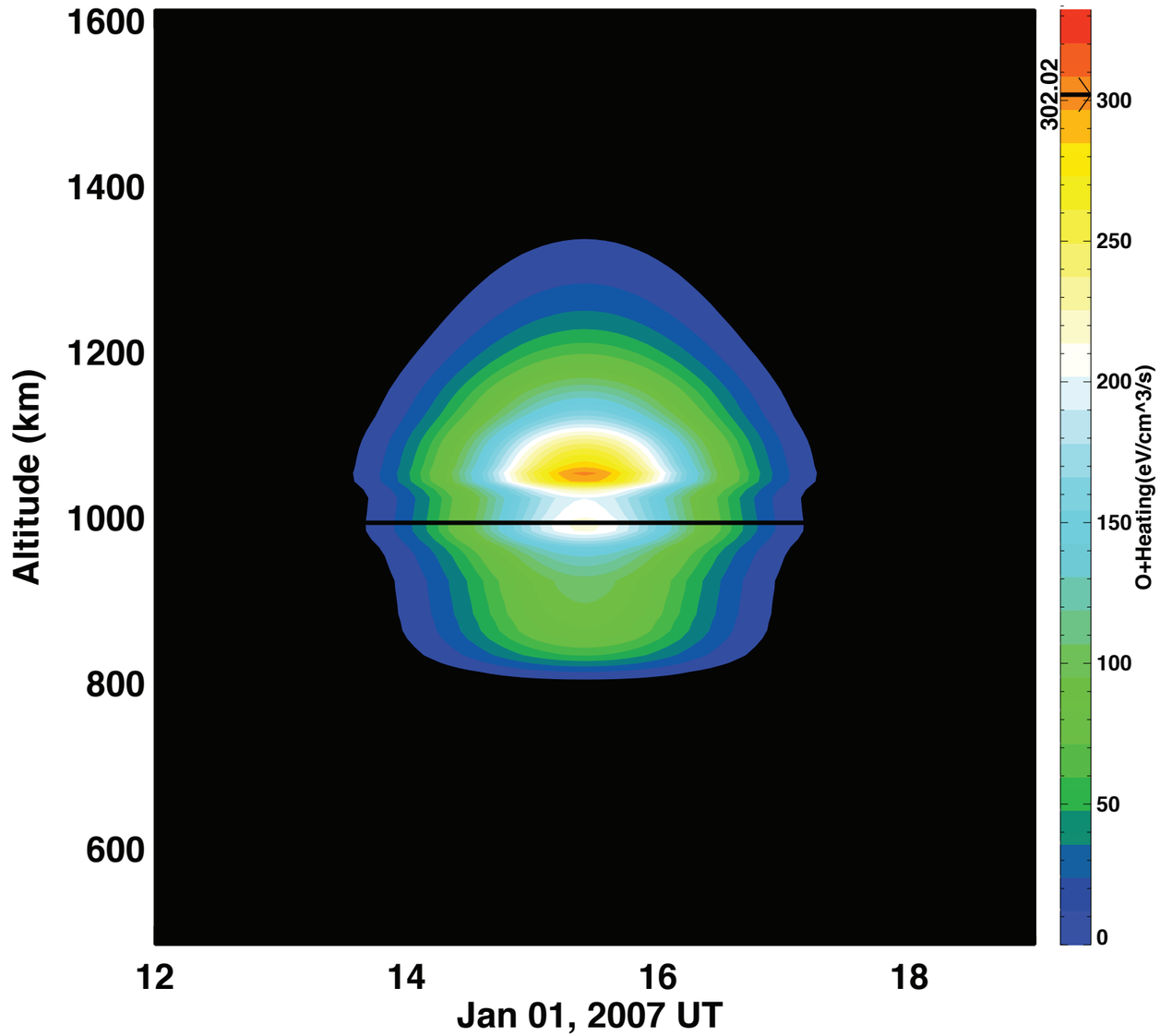
Altitude (km)
1600
1400
1200
1000
800
600
12
14
16
18
Jan 01, 2007 UT
302.02
300
250
200
150
100
50
0
O+Heating(eV/cm^3/s)

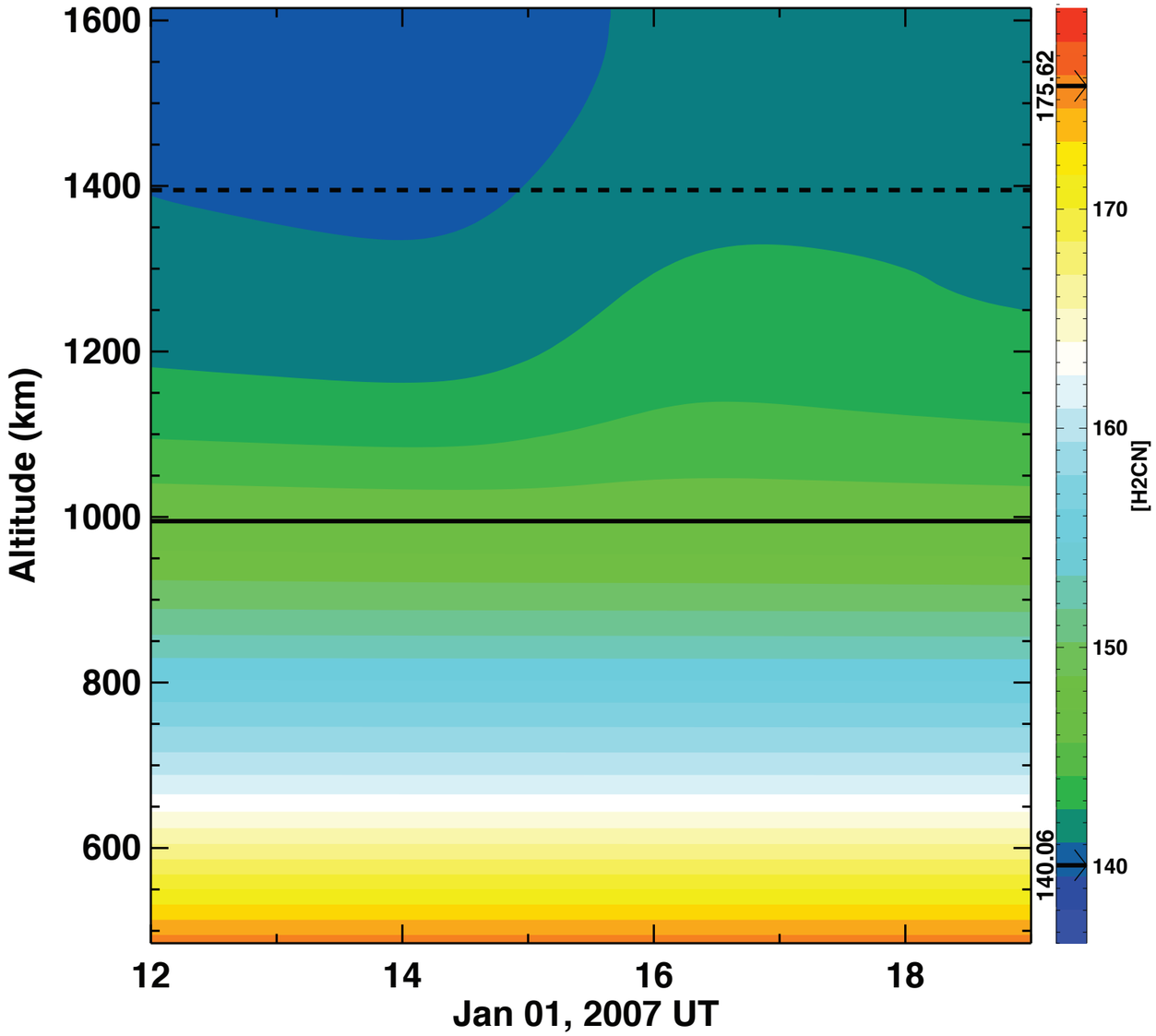
Altitude (km)
1600
1400
1200
1000
800
600
12
14
16
18
Jan 01, 2007 UT
175.62
170
160
150
140
140.06
[H2CN]

Figure 5.

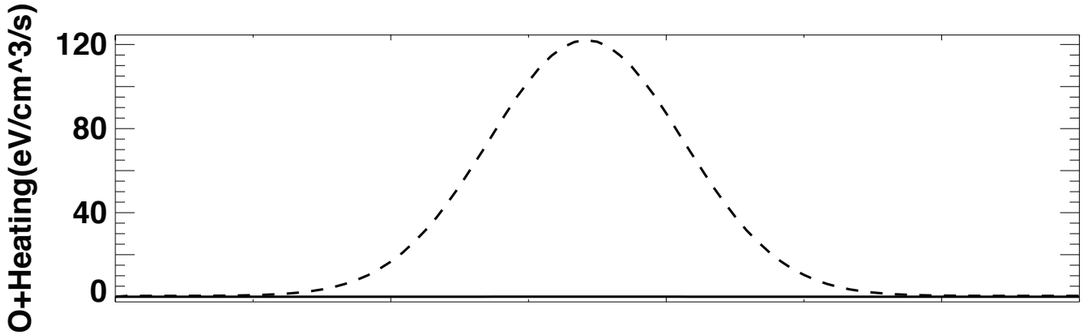
O+Heating(eV/cm^3/s)
120
80
40
0

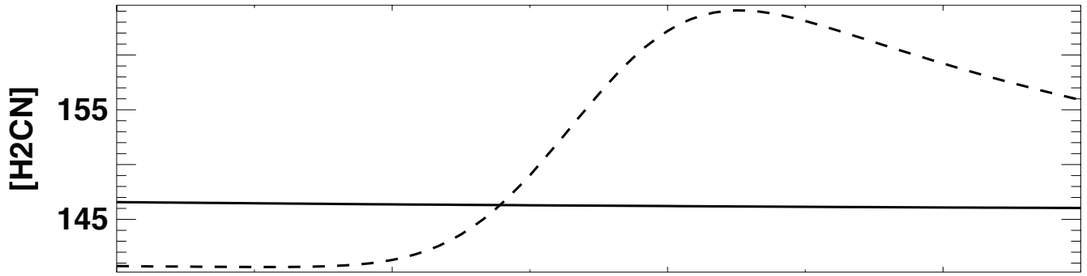
[H2CN]
155
145

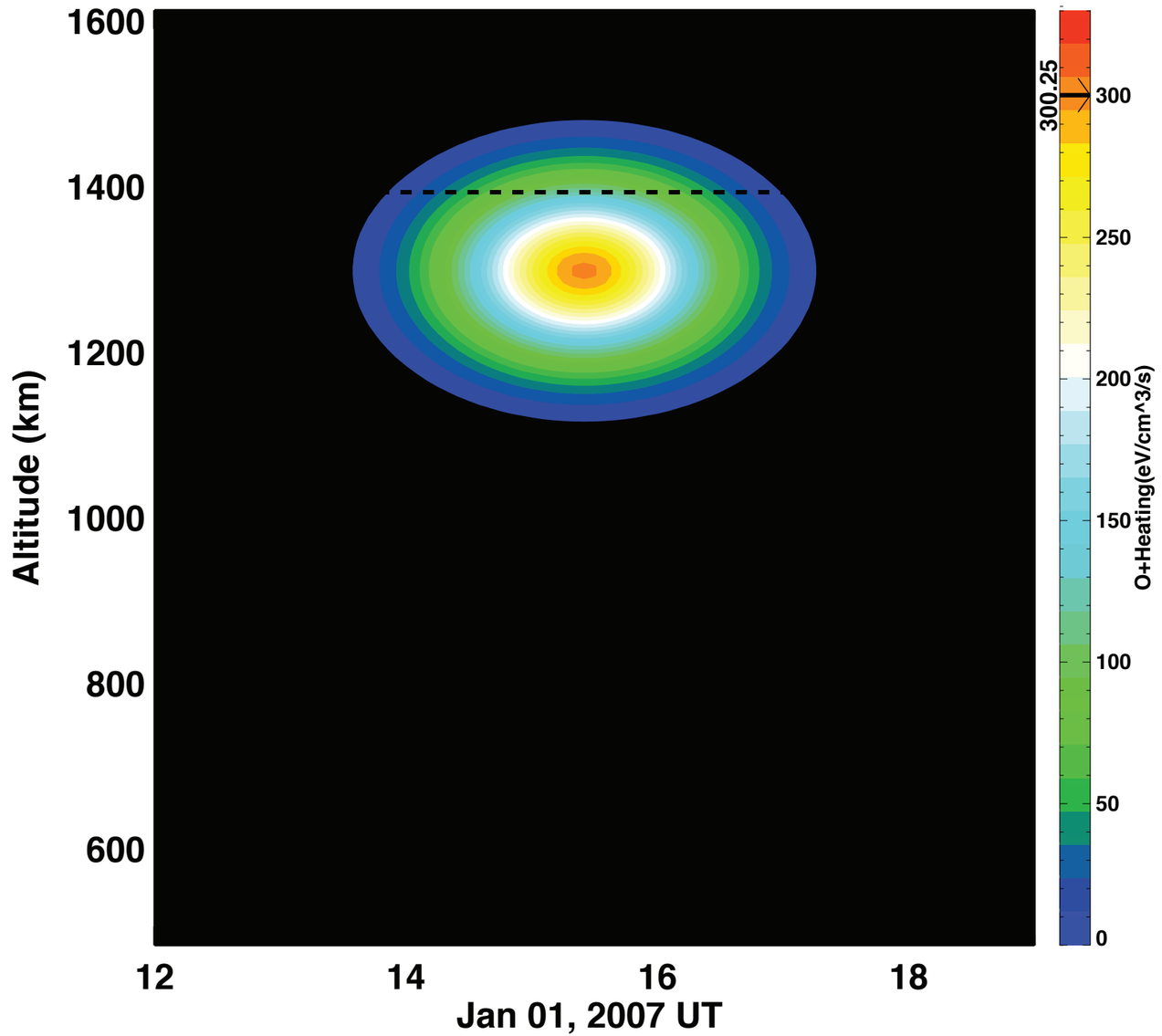
1600
1400
1200
1000
800
600
Altitude (km)
12
14
16
18
Jan 01, 2007 UT
300.25
300
250
200
150
100
50
0
O+Heating(eV/cm^3/s)

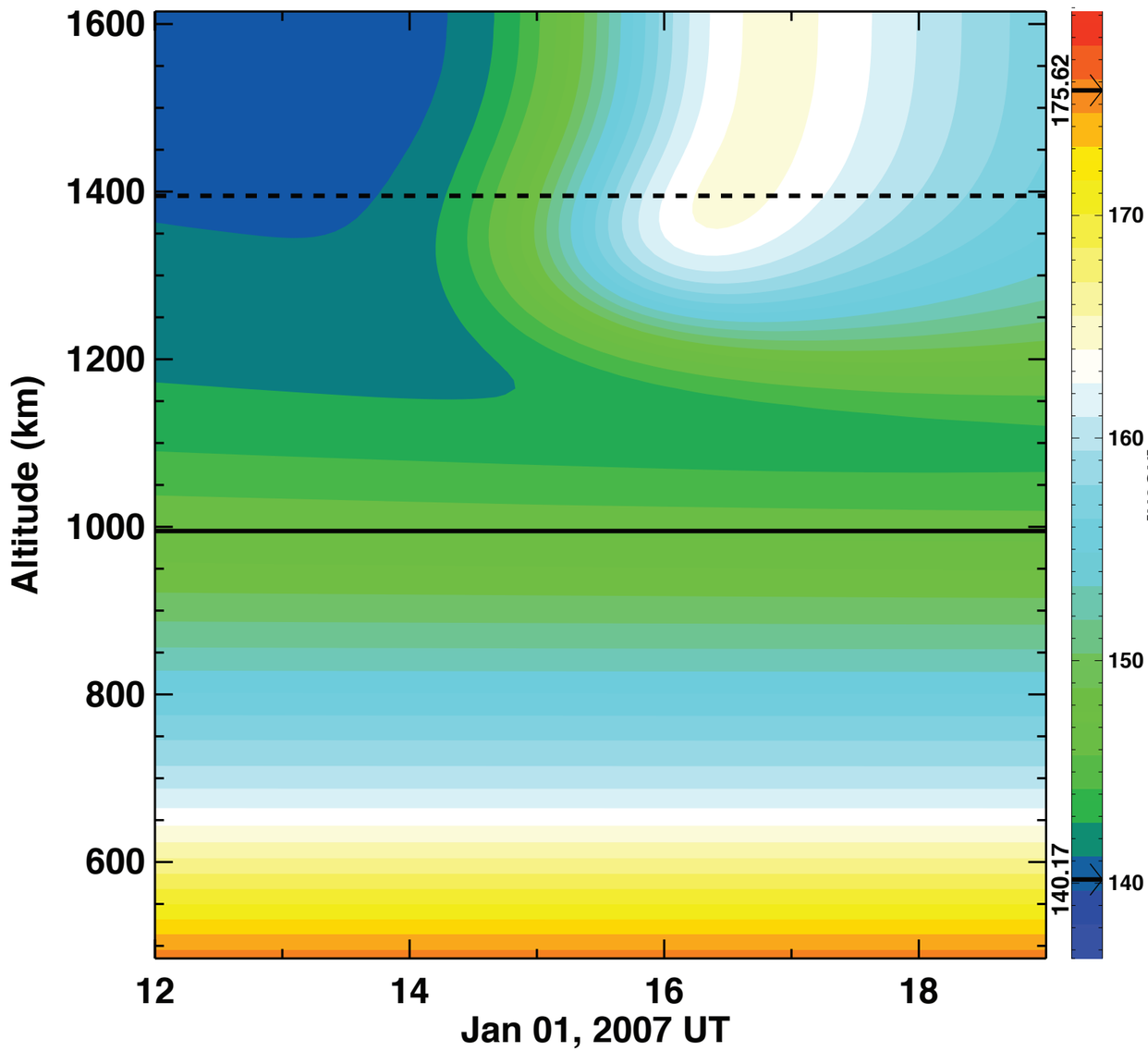
1600
1400
1200
1000
800
600
Altitude (km)
12
14
16
18
Jan 01, 2007 UT
175.62
170
160
150
140
140.17
[H2CN]